doi:10.1017/S1431927622002823
Microsc. Microanal. 28 (Suppl 1), 2022
© Microscopy Society of America 2022

Quantification of Contrast Difference Between Monoclinic and Tetragonal Zirconia in Low-kV SEM

Farzin A. Arpatappeh[1], Cleva Ow-Yang[1,2], Sorour Semsari Parapari[3], Gülcan Çorapçıoğlu[4], Mehmet Ali Gülgün[1,2*] and Melih Papila[1]

1. Sabancı University, Faculty of Engineering and Natural Sciences, Istanbul, Turkey.
2. Sabancı University, SUNUM Nanotechnology Research and Application Center, Istanbul, Turkey.
3. Jozef Stefan Institute, Ljubljana, Slovenia.
4. Koç University, Central Research Infrastructure Directorate, Istanbul, Turkey.
5. BaX Composites, Istanbul, Turkey.
* Corresponding author: mehmet.gulgun@sabanciuniv.edu

To address the challenge in differentiating between two different allotropes when imaging with secondary electrons in the SEM, we present a study in which we quantitatively interpreted the contrast in secondary electron images collected using a through-the-lens detector. We demonstrated this new quantitative approach on a sample containing both tetragonal zirconia (t-ZrO_2) and monoclinic zirconia (m-ZrO_2) that was imaged over an accelerating voltage range of 0.4 - 1 keV. These results complement the existing capabilities offered by TEM, EBSD, micro-Raman, and correlative Raman-secondary electron imaging.

Previous studies have used image contrast levels to differentiate between semiconductors, metals, alloys, organic structures, and ceramics arising from their inherent differences in composition. For example, in semiconductors, this method was used to the direct visualization of dopant types [1-5], mapping of dopant levels [6-8] and even for capturing the four-dimensional images of the carrier interface dynamics in p-n junctions [9,10]. In metals, fine grains of precipitates in a Cr-Mo steel were identified and visualized based on the difference in the secondary electron contrast [11]. In organic materials, compositional contrast of uncoated fungal spores and stained section-face was also imaged by this method [12]. In the case of ceramics, the results of investigations on composites such as BN/TiB_2, Si_3N_4/$MoSi_2$, and ZrO_2/Al_2O_3/Ti(C,N) using a low-voltage field-emission scanning electron microscope (FESEM) revealed a relationship between the phase contrast in the images and the local electrical conductivity, which made it possible to distinguish between grains that formed a three-dimensional conductive network from those grains which were isolated in the composite [13]. Percolated and non-percolated Ni phases were differentiated based on their difference in the SE yield in solid oxide fuel cells of Ni–yttria stabilized zirconia (ZrO_2) [14]. The contrast level differences were associated with physical properties, such as the variation in local conductivity, the difference in the secondary electron yield, and the difference of the bandgap width, due to the different electronic configurations. In this paper, we focus on the quantification and numerical analysis of the contrast difference originating in two distinct polymorphs of ZrO_2, i.e., of different crystal structures.

Partially stabilized tetragonal ZrO_2 doped with 3 mol% Y was obtained from TOSOH. Monoclinic zirconia was synthesized from zirconyl chloride octahydrate (Fluka) by calcination at 1000 ºC for 1 hour. Both powders were analyzed for their crystallographic structure using an XRD (Bruker D2 Phaser).

The two ZrO_2 powders were investigated using a FE-SEM (Zeiss Leo Supra 35 VP) with an accelerating voltage tunable between 150 V and 30 kV, with a step resolution of 10 V. The samples were sputter-

CrossMark

coated with a Au-Pd alloy of thickness *ca.* 4.38 nm. FE-SEM imaging was performed under a vacuum level of *ca.* 10^{-7} mbar and over accelerating voltages of 0.4 to 1 keV. The "in-lens" detector used preferentially collected Type I and Type II secondary electron signals (representative micrograph in Figure 1). This operation mode provided high resolution imaging with sensitivity to variations in the surface energy enabling correlation of electronic structure, work function, and crystal structure in materials with the observed contrast level in electron micrographs.

Images that included the two phases and the background were analyzed. Before processing, the images were prepared for analysis with an image editing software (GIMP). The two phases were singled out of the micrograph in the form of two separate phase images with the same size of the parent image, but all the areas except for the phases were set to be transparent (Figure 1). A Python® code was written to quantify the contrast difference between the m-ZrO_2 (m-phase) and t-ZrO_2 (t-phase), as a function of accelerating voltage.

The parent image and the phase images were analyzed to extract histograms of their intensity (Figure 2) in the range of grayscale level (GSL) of 0 (black) to 256 (white). In the case of phase images, the program interpreted the transparent area as a GSL = 0. After removing these values from the image matrix, the average grayscale level (AGSL) of the remnant part (solely the phase) was calculated. The difference in AGSL, designated as Δ_{AGSL}, was calculated by subtracting the AGSL of t-phase from that of m-phase. The percentage difference in AGSL was also calculated by divided by AGSL of m-phase. The standardized Δ_{AGSL} plotted versus electron acceleration voltage (Figure 3).

Figure 1 shows the representative micrograph of the secondary electron signals from both phases captured by the in-lens detector in 0.5 kV. There is a difference between the contrast levels in the electron micrograph so that m-phase appear brighter than the t-phase. When the same powders were captured in a range of acceleration voltages, it was revealed that the contrast difference increased as the acceleration voltage was decreased from 1 kV to 0.4 kV. The difference between the contrast levels of m-phase and t-phase is because of the difference in the SE yield of these phases.

Figure 1 also shows the processing steps of micrograph. The image shows two particles belonging to different phases and the way they were singled out in the form of m-phase and t-phase. The same parent electron micrograph and two submicrographs were analyzed using the computer code. Their histograms and processed images were presented in Figure 2. AGSL for the histograms of m-phase and t-phase are shown with a red dashed line.

Figure 3 shows the standardized Δ_{AGSL} between m-phase and t-phase against the acceleration voltage. It shows how the standardized Δ_{AGSL} monotonously increased as the acceleration voltage was reduced. The Δ_{AGSL} was about 2.81% when the acceleration voltage was 5 kV. Δ_{AGSL} starts to rise as the acceleration voltage was reduced. When the acceleration voltage was 0.4 kV, the standardized Δ_{AGSL} was to 69.2%.

This method appears to be a promising and feasible method for the differentiation of allotropes that would not be distinguishable in an SEM unless using complex equipment. This method can be further improved to distinguish even smaller grains of allotropes.

https://doi.org/10.1017/S1431927622002823 Published online by Cambridge University Press

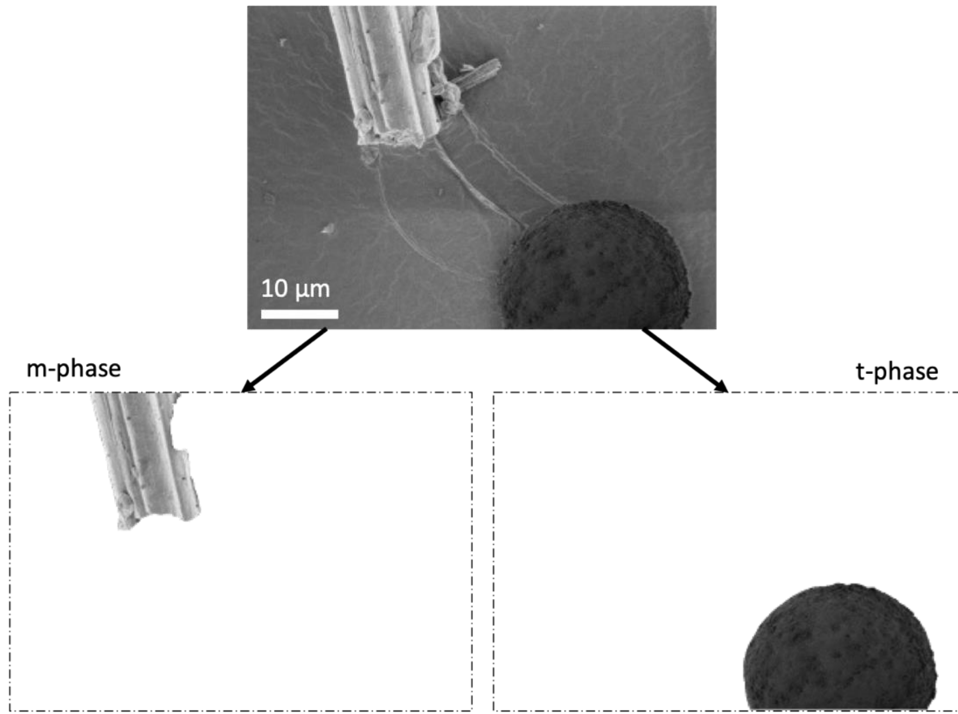

Figure 1. Manual segmentation of t-phase and m-phase from electron micrograph captured at 0.5 kV with an in-lens detector.

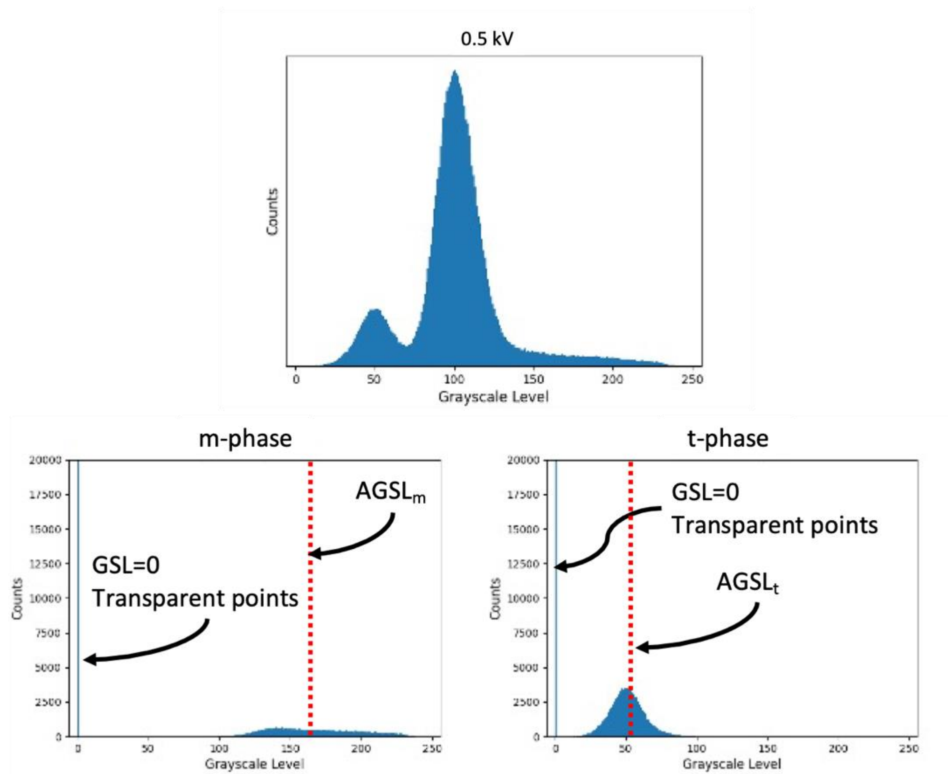

Figure 2. Histogram of grayscale levels for t-phase, m-phase and complete SEM micrograph captured with an in-lens detector at 0.5 kV.

https://doi.org/10.1017/S1431927622002823 Published online by Cambridge University Press

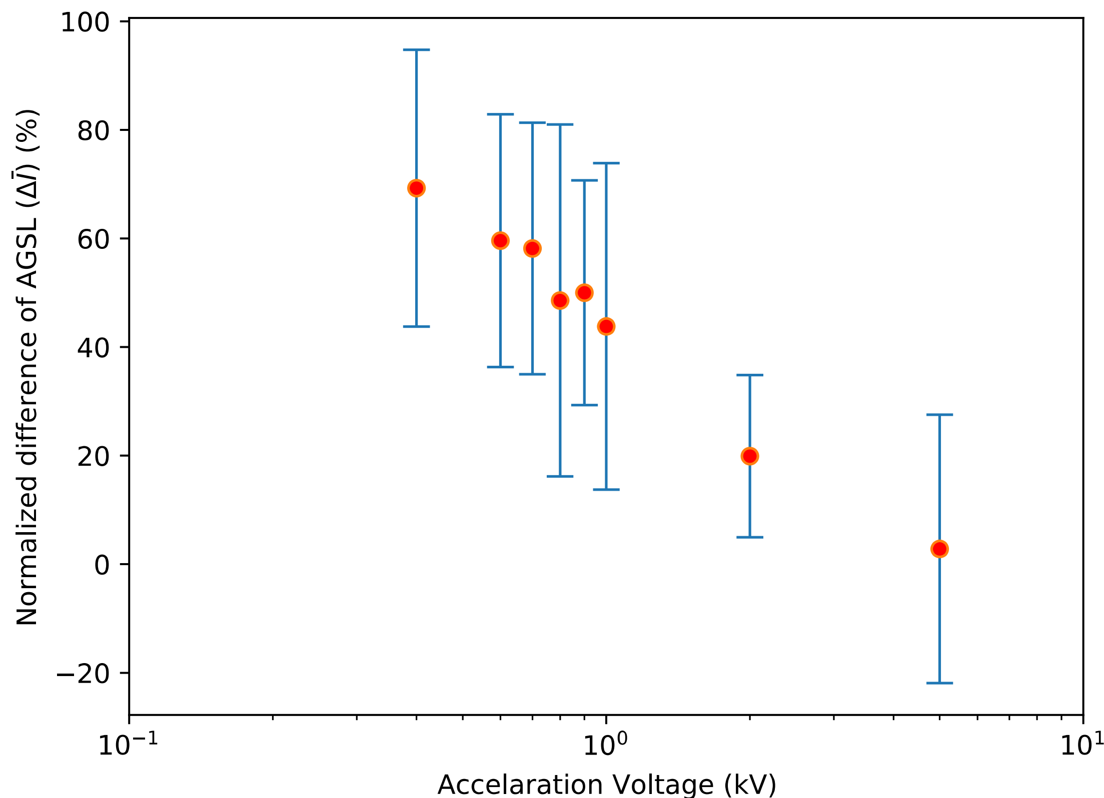

Figure 3. Standardized difference between the AGSL (right) for t-phase and m-phase in SEM micrographs captured with an in-lens detector in a range of acceleration voltages (5 - 0.4 kV).

References:

[1] DD Perovic et al., Ultramicroscopy **58** (1995), p. 104. doi: 10.1016/0304-3991(94)00183-N
[2] MR Castell et al., Ultramicroscopy **69** (1997), p. 279. doi: 10.1016/S0304-3991(97)00051-X
[3] MR Castell et al., Appl. Phys. Lett. **74** (1999), p. 2304. doi: 10.1063/1.123832
[4] I Jóźwik et al., Ultramicroscopy **228** (2021), p. 113333. doi: 10.1016/j.ultramic.2021.113333
[5] I Jóźwik et al., Mater. Sci. Semicond. Process. **138** (2022), p. 106293. doi: 10.1016/j.mssp.2021.106293.
[6] R. Turan et al., Appl. Phys. Lett. **69** (1996), p. 1593. doi: 10.1063/1.117041
[7] C. Schönjahn et al., J. Appl. Phys. **92** (2002), p. 7667. doi: 10.1063/1.1525862
[8] SL Elliott et al., J. Appl. Phys. **91** (2002), p. 9116. doi: 10.1063/1.1476968
[9] E. Najafi et al., Science **347** (2015), p. 164. doi: 10.1126/science.aaa0217
[10] J. Sun et al., J. Phys. Chem. Lett. **7** (2016), p. 985. doi: 10.1021/acs.jpclett.5b02908
[11] T. Nakamura et al., Mater. Trans. **60** (2019), p. 1591. doi: 10.2320/matertrans.M2019078
[12] KW Kim and H. Jaksch, Micron **40** (2009), p. 724. doi: 10.1016/j.micron.2009.05.001
[13] K Sempf et al., J. Eur. Ceram. Soc. **36** (2016), p. 3531. doi: 10.1016/j.jeurceramsoc.2016.05.034
[14] K Thydén et al., Solid State Ionics **178** (2008), p. 1984. doi: 10.1016/j.ssi.2007.12.075

https://doi.org/10.1017/S1431927622002823 Published online by Cambridge University Press